Accelerated convergence of convective simulations using boundary value problems

Evan H. Anders and Benjamin P. Brown
Dept. Astrophysical & Planetary Sciences, University of Colorado – Boulder, Boulder, CO 80309, USA and Laboratory for Atmospheric and Space Physics, Boulder, CO 80303, USA

Jeffrey S. Oishi
Department of Physics and Astronomy, Bates College, Lewiston, ME 04240, USA

We present a method for coupling Boundary value problems (BVPs) with Initial value problems (IVPs) in order to achieve thermally converged convective solutions on dynamical timescales, rather than the long thermal timescale. We demonstrate the similarity between the solution reached by BVP and the solution reached by a long thermal rundown of the IVP, and demonstrate that this method works at a large range of supercriticalities. We use this method to achieve converged solutions at high Ra, and discuss its extension to more complex scenarios, such as stratified, compressible convection.

I. INTRODUCTION

Natural convection occurs in the presence of disparate timescales. Granules on the solar surface overturn on the order of 10 minutes, whereas deep motions in the Sun are likely at low Mach number and constrained by the solar rotation rate of ∼1 month. Both of these dynamical timescales are vastly shorter than the Sun's average timescale of energy transport, which is the Kelvin-Helmholtz timescale of nearly 3×10^7 *years* [1]. As simulations aim to model natural convection by increasing into the high-Rayleigh Number (Ra) regime, where diffusive timescales are much longer than dynamical timescales [2], achieving converged simulations will require runs which span a greater number of convective timescales in order to thermally converge. Furthermore, with increasing Ra and decreasing diffusivities, motions become more turbulent and require finer grid meshes and shorter timesteps to resolve turbulent motions, increasing the simulation time required for each overturn timescale. These two effects conspire to make achieving thermally converged, high-Ra, astrophysically interesting simulations an intractable problem using modern numerical tools.

Prior studies of stratified convection in which a convective layer lies between stable layers have used the knowledge of Mixing Length Theory (MLT) to adjust the initial thermodynamic structure of the atmosphere to a state which is closer to the adiabat chosen by convection [3]. However, many modern studies of convection do not contain stable layers above and below the convection zone, and the presence of hard boundaries and the boundary layers that they form make it difficult to know the correct evolved adiabat *a priori*.

Here we present a method for using simple boundary value problems (BVPs), along with information about the evolved flow fields, to fast-forward the slow thermal evolution of convecting simulations. We run two sets of experiments: one in which we allow convective simulations to evolve for a full thermal timescale before taking measurements, and another in which we employ a fast, BVP technique which occurs on dynamical timescales. We compare these two sets of simulations to show the validity of the BVP technique. We use the BVP technique to run simulations at high Ra, in the regime where running for thermal timescales becomes computationally intractable.

II. EXPERIMENT

We adopt the Oberbeck-Boussinesq approximation. Under this choice, the fluid has constant kinematic viscosity (ν), thermal diffusivity (κ), and coefficient of thermal expansion (α). The variables of the fluid that are evolved are the velocity, $\boldsymbol{u} = u\hat{x} + v\hat{y} + w\hat{z}$, the temperature $T = T_0 + T_1$, and the pressure, P. The density of the fluid is a constant ρ_0, except on the term where the constant gravitational acceleration, $\boldsymbol{g} = -g\hat{z}$ acts in the vertical momentum equation, in which case it is $\rho = \rho_0(1 - \alpha T_1)$. Under these choices, the equations of motion are [4]

$$\nabla \cdot \boldsymbol{u} = 0, \tag{1}$$

$$\frac{\partial \boldsymbol{u}}{\partial t} + \boldsymbol{u} \cdot \nabla \boldsymbol{u} = -\frac{1}{\rho_0}\nabla P - g(1 - \alpha T_1)\hat{z} + \nu \nabla^2 \boldsymbol{u}, \tag{2}$$

$$\frac{\partial T_1}{\partial t} + \boldsymbol{u} \cdot \nabla (T_0 + T_1) = \kappa \nabla^2 T_1, \tag{3}$$

We non-dimensionalize these equations such that length scales are in units of the layer height (L_z), temperature is in units of the initial temperature jump across the layer ($\Delta T_0 = L_z \nabla T_0$), and time is in units of the freefall timescale ($L_z/v_{\rm ff}$), where the freefall velocity is $v_{\rm ff} = \sqrt{\alpha g L_z^2 \nabla T_0}$. We further re-arrange the momentum equation by introducing a reduced kinematic pressure, $\varpi \equiv P/\rho_0 + \phi + |\boldsymbol{u}|^2/2$, where $\boldsymbol{g} = -\nabla\phi$ is the gravitational potential. Despite containing a nonlinear $\boldsymbol{u}$ component, the nature of P in Rayleigh-Bénard convection, as a Lagrange multiplier, allows us to treat ϖ as a linear unknown, without a need to resolve its different components. We time evolve the equations in the form,

$$\nabla \cdot \boldsymbol{u} = 0, \tag{4}$$

$$\frac{\partial \boldsymbol{u}}{\partial t} + \nabla\varpi - T_1\hat{z} + \mathcal{R}\nabla\times\boldsymbol{\omega} = \boldsymbol{u}\times\boldsymbol{\omega} \tag{5}$$

$$\frac{\partial T_1}{\partial t} - \mathcal{P}\nabla^2 T_1 + w\frac{\partial T_0}{\partial z} = -\boldsymbol{u}\cdot\nabla T_1, \tag{6}$$

where $\boldsymbol{\omega} = \nabla\times\boldsymbol{u}$ is the vorticity. We find Eq. (5) to be slightly faster numerically than the standard form in Eq. (2). The dimensionless control parameters are set by the Rayleigh and Prandtl numbers,

$$\mathcal{R} \equiv \sqrt{\frac{\rm Pr}{\rm Ra}}, \qquad \mathcal{P} \equiv \frac{1}{\sqrt{\rm Pr\,Ra}}, \qquad {\rm Ra} = \frac{g\alpha L_z^4 \nabla T_0}{\nu\chi} = \frac{(L_z\, v_{\rm ff})^2}{\nu\chi}, \qquad {\rm Pr} = \frac{\nu}{\chi}. \tag{7}$$

The dimensionless vertical extent of the domain is $z = [-1/2, 1/2]$, and at the boundaries we impose no-slip, impenetrable boundary conditions such that $w = u = v = 0$ at $z = \pm 1/2$. At the lower boundary, we employ a fixed flux condition such that $\partial T_1/\partial z = 0$ at $z = -1/2$, and we impose a fixed temperature condition $T_1 = 0$ at $z = 1/2$. Both horizontal directions are periodic, extending over a range $x, y = [0, \Gamma]$, where the aspect ratio is $\Gamma = 2$. In our 2D cases, we only examine the x and z dimensions and we set $v = \partial_y = 0$.

The chosen thermal boundary conditions at the upper and lower plates determine key quantities of the evolved state. Studies of incompressible, Boussinesq, Rayleigh-Bénard convection often employ fixed temperature (Dirichlet) or fixed heat flux (Neumann) boundary conditions at both plates. Dirichlet conditions represent plates of infinite conductivity, whereas Neumann conditions model plates of finite conductivity. In both cases, choosing symmetric boundary conditions maintains overall system symmetry, and despite evolving towards different thermal structures, both types of conditions transport heat in the same manner [5]. Studies of convection which aim to model astrophysical systems such as stars often employ a mixture of these two types of boundary conditions [6–8]. The flux at the lower boundary is fixed, modeling the constant energy generation of the stellar core, while the outer boundary condition is held at a fixed temperature, modeling the surface of a star which must output the energy generated internally. This setup is a useful model for understanding natural systems, but simulations which employ these boundary conditions suffer from a long thermal relaxation as the atmosphere loses energy and approaches the adiabat chosen by the Dirichlet condition. We choose these conditions in part to better understand them, and in part because these conditions minimize the number of assumptions that must be made in setting up the boundary value problem. For this choice of boundary conditions, the critical Ra is ${\rm Ra}_{\rm crit} = 1295.78$, and we will often speak in terms of the supercriticality, $S = {\rm Ra}/{\rm Ra}_{\rm crit}$.

A. The Boundary Value Problem

It is reasonable to assume that convection will evolve the mean temperature profile that drives it over the course of a thermal diffusion time, $t_\chi = \mathcal{P}^{-1}$. Thus, as Ra increases, the timescale for achieving a thermally converged mean temperature profile becomes intractable. This prohibitively long thermal timescale in an Initial Value Problem (IVP) can be skipped by coupling the IVP with a simple Boundary Value Problem (BVP) solve. By using information about the convecting dynamical state of an unconverged solution, a BVP can be used to solve for the evolved system state. A comparison of a simulation running for the thermal timescale, and another where a BVP is used to fast-forward atmospheric evolution, are shown in Fig 1a&b.

The Boussinesq BVP in essence contains equations of hydrostatic balance and thermal equilibrium,

$$\frac{\partial}{\partial z}\langle\varpi\rangle - \langle T_1\rangle\hat{z} = \langle\boldsymbol{u}\times\boldsymbol{\omega}\rangle, \tag{8}$$

$$\frac{\partial}{\partial z}\langle wT_1\rangle - \mathcal{P}\frac{\partial^2}{\partial z^2}\langle T_1\rangle = 0, \tag{9}$$

where $\langle A\rangle$ represents a time- and horizontally averaged profile of the quantity A. These equations arise from assuming that the atmosphere is in a steady state ($\partial_t \to 0$), then taking time and horizontal averages of Eqns (5&6) and

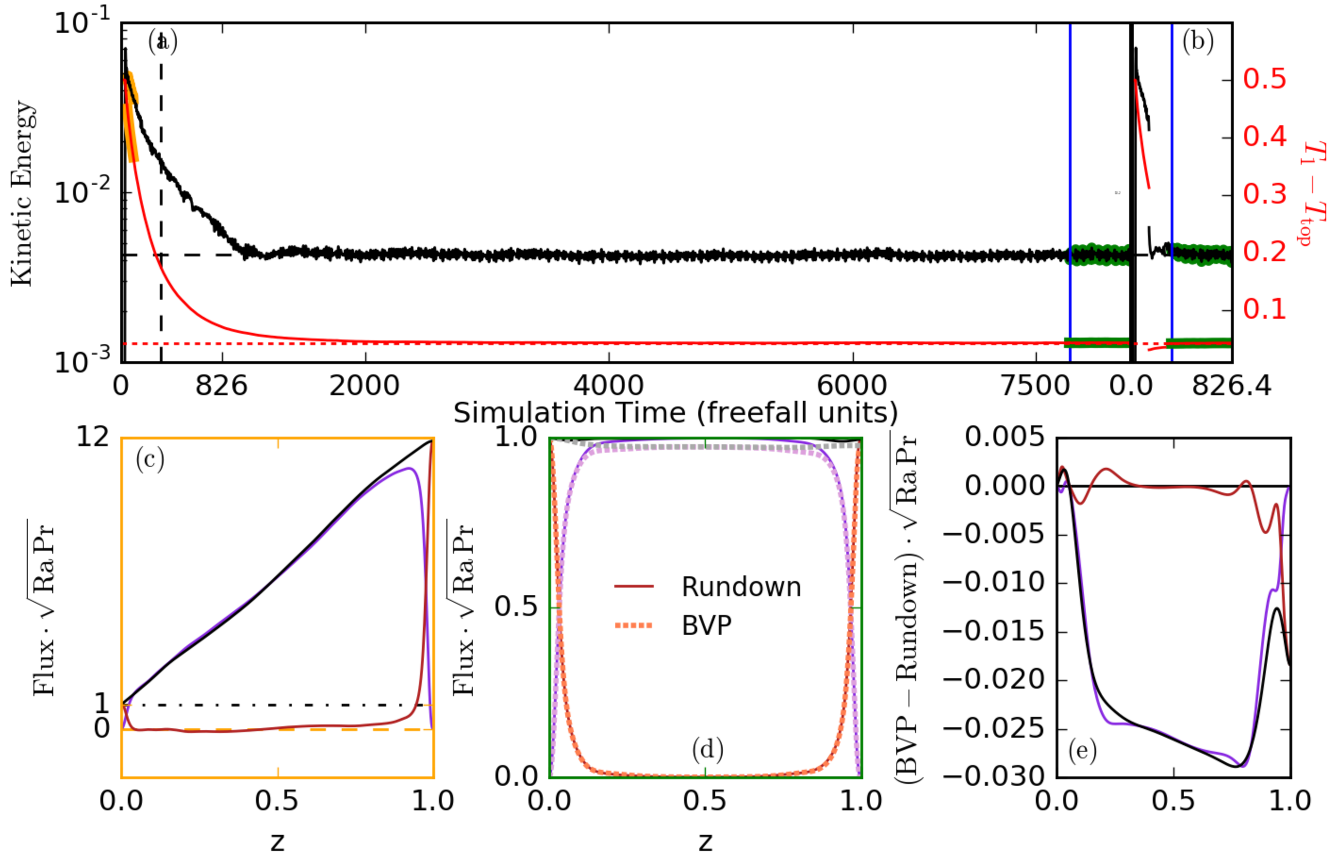

FIG. 1. Traces of system energies vs. time for a long thermal rundown (a) and BVP convergence (b) are shown for $S = 10^{4+2/3}$. The horizontal extent of the subplots is set such that one simulation time unit takes up an equal amount of paper space in (a) and (b). Volume averaged kinetic energy is shown in black, and the volume averaged temperature with the top value removed, is shown in red. The dashed vertical line on (a) represents the time at which averaging begins in the BVP solution in (b), and the horizontal dashed lines show the equilibrium value of the energies. The blue vertical lines represent the beginning of the time-averaging window. (c) System fluxes early in the run (the orange highlights in (a)) are shown. Black is the sum of the flux, purple is the convective flux, and red is the conductive flux. (d) Fluxes in the converged rundown IVP compared to the converged BVP. The sum of flux is shown in black & grey, the convective flux is shown in purple & pink, and the conductive flux is shown in red & orange. (e) The differences between the BVP and rundown fluxes is shown. While not in perfect agreement, the BVP fluxes deviate from the rundown fluxes by only a few percent of the total flux, and are much closer to the converged state than the initial fluxes, as in (c).

neglecting terms that vanish due to the symmetry of the problem. Convective flows are perturbations around a thermal profile defined by these equations in the proper evolved, statistically stationary state.

Under eqns (8&9), the thermal structure ($\langle T_1 \rangle$, $\langle \varpi \rangle$) of the atmosphere is fully determined by the specification of two profiles: the convective flux, $F_{conv} = \langle w T_1 \rangle$, and the nonlinear advection, $\langle \boldsymbol{u} \times \boldsymbol{\omega} \rangle$. If these profiles are known, then solving for $\langle T_1 \rangle$ and $\langle \varpi \rangle$ depends only upon the choice of boundary conditions.

By definition, the profile of $F_{\rm conv}$ is not in a time stationary state early in the IVP. In fact, as the atmosphere approaches the isotherm specified by the upper (fixed T) boundary condition, the motions display an asymmetric flux as energy leaks through the upper boundary condition (Fig. 1c) in order to reach a lower temperature state. In order to construct the evolved convective flux from the current fluxes in the atmosphere, we assume that the atmospheric dynamics have properly developed the thickness of the boundary layers. In other words, if we know the quantities $F_{\rm conv}$, $F_{\rm cond} = \langle -P \partial_z T \rangle$, and $F_{\rm tot} = F_{\rm conv} + F_{\rm cond}$, we assume that the profiles

$$f_{\rm conv}(z) = \frac{F_{\rm conv}}{F_{\rm tot}}, \qquad f_{\rm cond}(z) = \frac{F_{\rm cond}}{F_{\rm tot}} \tag{10}$$

early in the evolution are the same as they will be in the final steady state solution. By definition, the evolved total flux through the atmosphere must be the same as the flux entering the atmosphere at the bottom boundary,

$F_{\text{tot, steady}} = F_{\text{bot}}$. The proper convective flux profile to use in Eqn. (9) is then $\langle wT_1\rangle_{\text{steady}} = F_{\text{tot, steady}} \cdot f_{\text{conv}}$.

In order to carry the converged amount of flux appropriately, the velocity field and temperature fluctuations in the system must be scaled by a quantity $\xi(z) = \langle wT_1\rangle_{\text{steady}} / \langle wT_1\rangle$. Thus, we multiply the velocities and the thermal fluctuations, $T - \langle T\rangle$, by $\sqrt{\xi}$, such that the product of all fluctuations (which carry the convective flux) are diminished by a factor of ξ. This also means that $\langle \boldsymbol{u} \times \boldsymbol{\omega}\rangle_{\text{steady}} = \xi \langle \boldsymbol{u} \times \boldsymbol{\omega}\rangle$. Once these profiles are appropriately adjusted, they can be used in the BVP solve to find $\langle T\rangle$ and $\langle \varpi\rangle$.

In general, the BVP solve is completed in the following steps:

1. Run the convective IVP. Once the convection achieves a volume-averaged Re of $\sqrt{\text{Ra}/\text{Ra}_{\text{crit}}}$, wait for 50 freefall time units.

2. Start taking the averages of F_{conv}, F_{tot}, and $\langle \boldsymbol{u} \times \boldsymbol{\omega}\rangle$, waiting either 30 freefall time units or until the average profiles change by no more than 1 part in 1000 on a given timestep, whichever is a more difficult criterion. This ensures that the profiles being used in the BVP are steady and smooth, and that they sample the full behavior of the convection.

3. Construct $\langle wT_1\rangle_{\text{steady}}$, ξ, and $\langle \boldsymbol{u} \times \boldsymbol{\omega}\rangle_{\text{steady}}$ from the flux profiles.

4. Solve for $\langle T_1\rangle$ and $\langle \varpi\rangle$ of the evolved state. Adjust the mean profiles in the IVP.

5. Multiply the velocity field and the fluctuations in T_1 about its horizontal average by $\sqrt{\xi}$ in the IVP.

6. Continue running the IVP for freefall 50 time units to allow for the velocities to equilibrate to their new background state.

7. Repeat steps 2-6 to complete a second BVP and get closer to the right solution now that we are far from the very unstable transient period.

8. Take averages for the amount of time specified for the given run in Appendix A.

B. Numerics

We utilize the Dedalus[1] pseudospectral framework [9] to time-evolve (4)-(6) using an implicit-explicit (IMEX), third-order, four-step Runge-Kutta timestepping scheme RK443 [10]. The temperature field is decomposed as $T = T_0(z) + T_1(x, y, z, t)$ and the velocity is $\boldsymbol{u} = w\hat{\boldsymbol{z}} + u\hat{\boldsymbol{x}} + v\hat{\boldsymbol{y}}$. In our 2D runs, $v = 0$. Variables are time-evolved on a dealiased Chebyshev (vertical) and Fourier (horizontal, periodic) domain in which the physical grid dimensions are 3/2 the size of the coefficient grid.

As initial conditions, we fill T_1 with random white noise whose magnitude is $10^{-6}(\text{Ra Pr})^{-1/2}$. This ensures that the initial perturbations are much smaller than the evolved convective temperature perturbations, even at large Ra. We filter this noise spectrum in coefficient space, such that only the lower 25% of the coefficients have power.

III. RESULTS

While Fig. 1 shows us that the post-BVP and post-rundown solutions exhibit similar system energies and fluxes, it is important to examine other aspects of the evolved solution. The BVP mainly serves to adjust the thermodynamic state of the solution; in Rayleigh-Bénard convection, this means that the evolved temperature profile is a good measure of whether or not the BVP achieves the proper solution.

The temperature profiles of a 2D run at $S = 10^{4+2/3}$ for both the BVP solve and the long rundown are shown in Fig. 2a. While they are not perfectly aligned they are within less than 0.25% of each other throughout the depth of the atmosphere, as shown in Fig. 2b. While the mean temperature profile is interesting, the point-by-point fluctuations in the temperature are what lead to convective transport, and thus examining the spread of temperature and the allowed values that it can take are important to characterizing the system. As seen in Fig. 2c, aside from the noticeable difference in the mode of the temperatures, the two runs exhibit largely the same spread of temperatures. (AUTHOR NOTE: I'll run a Kolmogorov-Smirnov test to compare the PDFs, but I need to collaborate on this to make sure that what I'm planning on doing makes sense – we should talk about this.)

---

[1] http://dedalus-project.org/

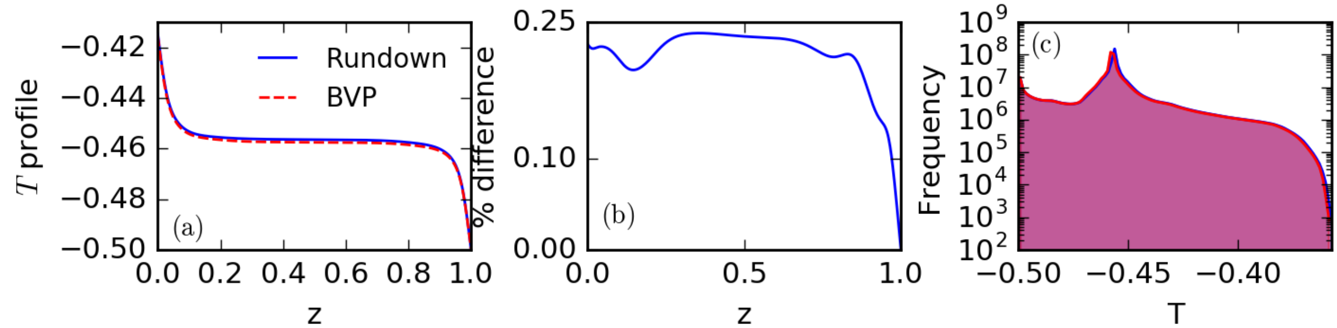

FIG. 2. Comparisons of the evolved thermodynamic states of a BVP solution and a long IVP rundown at $S = 10^{4+2/3}$ are shown. (a) Evolved temperature profiles, as a function of height. (b) The percentage difference between the temperature profiles (as shown in (a)), as a function of height. (c) Frequency distributions of point-by-point measurements of T throughout the two domains over the averaging windows are shown. The BVP shows excellent agreement with the thermal rundown (AUTHOR NOTE: I need to perform quantitative PDF comparisons, still).

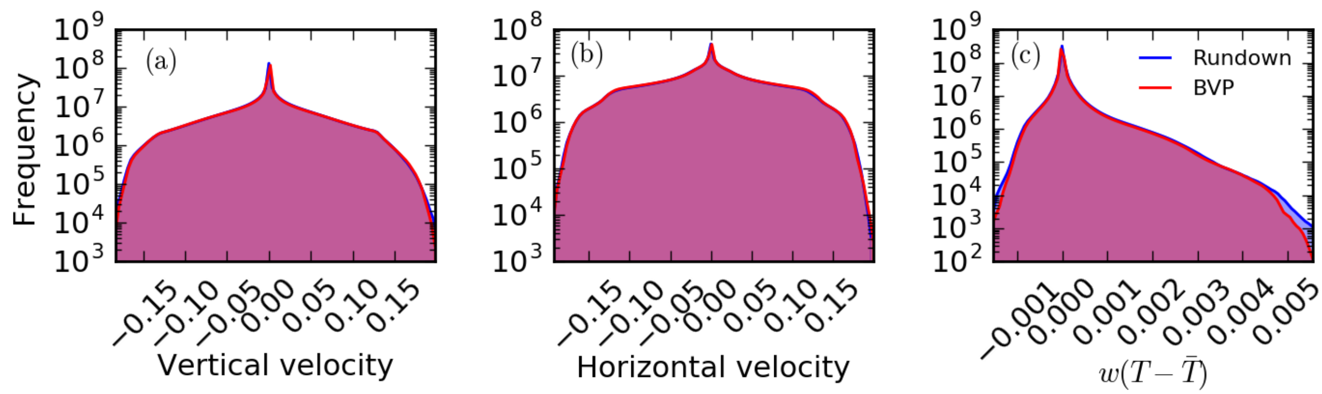

FIG. 3. Frequency distribution functions of the vertical velocity (a), horizontal velocity (b), and nonlinear vertical transport (c) are shown for a 2D run at $S = 10^{4+2/3}$. We sample flows every 0.1 time units for 500 freefall times, and include the flows at all points on the grid at each of these samples in these distributions. All distributions are biased by the no-slip, impenetrable boundary conditions, coupled with the dense spacing of our Chebyshev grids near the boundaries, so there is a large peak around zero. The distributions, and thus the nonlinear dynamics, are broadly similar, but they (maybe?) do not pass a two-tailed Kolmogorov-Smirnov similarity test. (AUTHOR NOTE: I just revamped the BVP method a bit on 1/12/2018, so I haven't had the time to run full tests on all the plots here)

In addition to examining the thermodynamics of the solutions, we are especially interested in determining if the post-BVP solution appropriately captures key features of the nonlinear dynamics. We show point-by-point frequency distributions of the horizontal velocity, vertical velocity, and nonlinear transport in Fig. 3. All of these measures have a sharp peak at zero due to the no-slip, impenetrable boundary conditions and the denser grid sampling near the boundaries of our Chebyshev grid. Regardless, we see that the velocities of the two solutions are largely consistent. The nonlinear transport in Fig. 3 shows that the rundown solution experiences more extreme events which carry a large amount of flux than the BVP solution, but the distributions are largely consistent. (AUTHOR NOTE: see previous paragraph comment).

The goodness of this method has been tested across a broad range of supercriticality. We have examined both Rundown and BVP solutions in the range $S = [10^{1/3}, 10^5]$ in 2D and $S = [10^1, 10^4]$ in 3D (3D points to come). We have also further explored up to $S = 10^6$ (AUTHOR NOTE: should we go up to 10^8? 10^7 is easily in reach. Also, 3D data points are sparse and will change – need to rerun with proper BVP procedure). We compare scalar, volume-averaged measurements of all of these runs in Fig. 4.

In Fig. 4a, we compare the Nusselt number scaling in 2D, 3D, and for BVP and rundown solutions. We use a

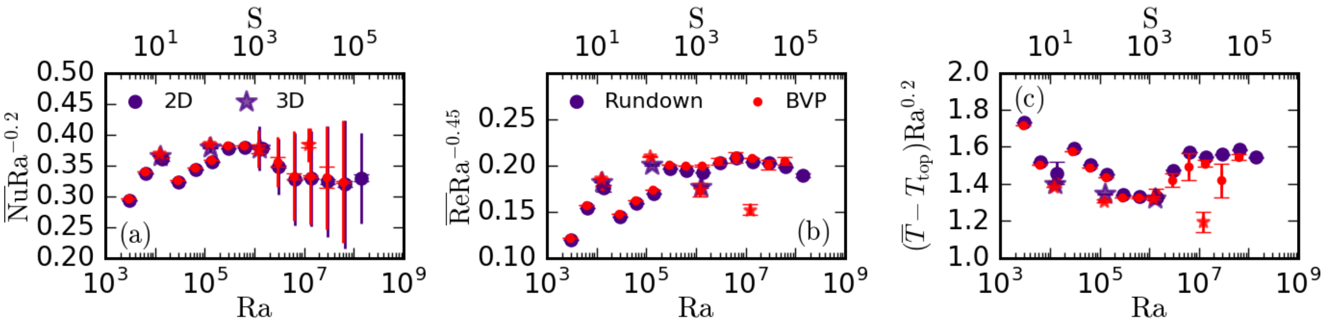

FIG. 4. Compensated scaling plots are shown for the Nusselt number (a), the Reynolds number (b), and the volume-averaged temperature (c). All plots are linear(y)-log(x), and any differences vertically are generally small. Symbols represent the mean value of a measurement, vertical lines represent the standard deviation of the measurement over the time window, and error bars represent the shift in the mean value over the window. All data points are staggered slightly off of their original value in the x-direction so as to show clearly the values of overlapping points at the same value of Ra. (a) Nu, which measures heat transport, scales roughly like $Ra^{1/5}$, and above Ra$\geq 10^6$, simulations display horizontally oscillating plumes which have oscillating periods of high transport and low transport. The mean value is marginally diminished as a result, and the variance of Nu with time is large. (b) Re, which measures the level of turbulence in the evolved solution, scales as Ra$^{0.45}$ in 2D and (something else?) in 3D. (c) The average temperature flucutation, minus the top temperature, which is a scalar measure of the final average thermodynamic state and should approach zero in the limit of infinitely large Ra. The temperature profile is slow to adjust, and differences between BVP solutions and rundown solutions are quite easy to pick out in this measure.

classic definition of the Nusselt number to measure the heat transport in these systems, where

$$\mathrm{Nu} = \frac{\langle F_{\mathrm{conv}} + F_{\mathrm{cond}} \rangle}{\langle F_{\mathrm{cond,\ ref}} \rangle} = \frac{\left\langle wT - (\mathrm{Ra\ Pr})^{-1/2}\nabla T \right\rangle}{\left\langle -(\mathrm{Ra\ Pr})^{-1/2}\nabla T \right\rangle}. \tag{11}$$

At small values of S, we achieve a steady state solution with a clear value of Nu. Near $S \sim 10^3$, our simulations begin to achieve a horizontally oscillatory state. Due to the use of no-slip boundaries, these states never give way to full scale shearing states, but they do reduce the overall heat transport through the system and cause the systems to oscillate between periods of high- and low- heat transport. The vertical lines represent the standard deviation of Nu associated with these oscillations, while the error bars show the drift of the mean value of Nu over the averaging window. We find that Nu $\propto$ Ra$^{1/5}$, a weaker scaling law than that seen in traditional Rayleigh-Bénard convection [5], but similar to that seen in shearing states [cite Goluskin]. (AUTHOR NOTE: Ben, I think this is entirely because of the oscillatory states. I wonder what would happen if we included viscous fluxes...)

In Fig. 4b, we measure the rms Reynolds number, where Re $= \langle |\boldsymbol{u}| \rangle / \mathcal{R}$. We find that this scales roughly as Re $\propto$ Ra$^{0.45}$, and find good agreement between BVP and rundown solutions.

In Fig. 4c, we measure the volume averaged temperature of our solution, then subtract out the value at the upper (fixed T) boundary. If the atmosphere were perfectly isothermal, this value would be exactly zero. Thus, this is a measure of the temperature jump across the boundary layers, and it provides insight both into whether or not the temperature profiles of two runs are the same and into whether the fluxes through the two systems are the same (it is in some ways an alternate measure of Nu [cite King 2009 supp materials]). We find that this measure is $\propto$ Ra$^{-1/5}$, approaching zero, as expected.

IV. DISCUSSION & CONCLUSIONS

The method presented here is a first step towards taking meaningful measurements of highly turbulent convection on manageable, human timescales. As demonstrated in Figs. 1-4, this BVP method quickly converges simulations to within a few percent of the true final state. Furthermore, the total simulation time required to use the BVPs does not change drastically from low S to high S, so the main prohibition on high Ra states is the difficulty of timesteps becoming increasingly small as turbulence increases. Additionally, post-BVP, we generally see an increase of the timestep size by nearly a factor of two due to the less intense driving of the near-converged state that is achieved quickly.

One major benefit of the BVP method used here is that it preserves the natural behavior of the convective solution (such as the horizontally oscillatory rolls of high-Ra 2D states in Fig. 4). One frequently used method of measuring dynamics in high-Ra simulations is that of bootstrapping, in which the converged solution of a low-Ra state is used as initial conditions for a higher-Ra simulation. While this method is powerful, it can be influenced by hysteresis effects, and the steady rolls achieved at low Ra can result in an artifically over-stable high-Ra roll solution. The BVP method we present here uses random noise initial conditions which allows the convective solution to naturally choose the dynamics.

Another benefit of our BVP method is that it can be easily extended to more complicated configurations. For example, to use this method in simulations of stratified compressible convection, one need only adapt the BVP equations to the appropriate equations of hydrostatic equilibrium and thermal equilibrium obtained by averaging the fully compressible, ideal gas steady state momentum and energy equations [2, 11]. In compressible convection, where the density is allowed to change, it is also essential to conserve mass by adding boundary conditions on the integrated mas density at the upper and lower boundaries, much as stellar structure codes do [12].

While we have not chosen to use them here, this BVP method can be extended to other boundary conditions. To solve for fixed temperature boundary conditions, the main difficulty is in finding the amount of flux through the system, $F_{\text{tot, steady}}$. However, by knowing the averaged value of the conductive flux (from the boundary conditions) and the ratios in Eqn. (10), $F_{\text{tot, steady}}$ can be found. In the case of fixed flux boundary conditions, the temperature solution is degenerate. However, using knowledge about the system – such as the initial symmetry of the RB state around $T = 0$, the final solution can be pegged onto the proper profile.

Future work will aim to apply the methods presented here to compressible systems, internally heated systems, and systems with more complex forms of the conductive flux.

ACKNOWLEDGMENTS

EHA acknowledges the support of the University of Colorado's George Ellery Hale Graduate Student Fellowship. This work was additionally supported by NASA LWS grant number NNX16AC92G. Computations were conducted with support by the NASA High End Computing (HEC) Program through the NASA Advanced Supercomputing (NAS) Division at Ames Research Center on Pleiades with allocations GID s1647 and GID g26133.

Appendix A: Table of Runs

S	Ra	nz	nx, ny	t_{therm}	t_{avg}	$\text{Nu}_{\text{rundown}}$	Nu_{BVP}
$10^{1/3}$	$2.79 \cdot 10^3$	32	128	52.8	100	(TBD)	(TBD)
$10^{2/3}$	$6.01 \cdot 10^3$	32	128	77.6	100	–	–
10^1	$1.30 \cdot 10^4$	32	128	114	100	–	–
$10^{1+1/3}$	$2.79 \cdot 10^4$	32	128	167	100	–	–
$10^{1+2/3}$	$6.01 \cdot 10^4$	32	128	245	100	–	–
10^2	$1.30 \cdot 10^5$	64	256	360	100	–	–
$10^{2+1/3}$	$2.79 \cdot 10^5$	64	256	528	100	–	–
$10^{2+2/3}$	$6.01 \cdot 10^5$	64	256	776	100	–	–
10^3	$1.30 \cdot 10^6$	128	512	$1.14 \cdot 10^3$	200	–	–
$10^{3+1/3}$	$2.79 \cdot 10^6$	128	512	$1.67 \cdot 10^3$	500	–	–
$10^{3+2/3}$	$6.01 \cdot 10^6$	256	1024	$2.45 \cdot 10^3$	500	–	–
10^4	$1.30 \cdot 10^7$	256	1024	$3.60 \cdot 10^3$	500	–	–
$10^{4+1/3}$	$2.79 \cdot 10^7$	256	1024	$5.28 \cdot 10^3$	500	–	–
$10^{4+2/3}$	$6.01 \cdot 10^7$	256	1024	$7.76 \cdot 10^3$	500	–	–
10^5	$1.30 \cdot 10^8$	512	2048	$1.14 \cdot 10^4$	500	–	–
$10^{5+1/3}$	$2.79 \cdot 10^8$	512	2048	$1.67 \cdot 10^4$	500	–	–
$10^{5+2/3}$	$6.01 \cdot 10^8$	512	2048	$2.45 \cdot 10^4$	500	–	–
10^6	$1.30 \cdot 10^9$	1024	4096	$3.60 \cdot 10^4$	500	–	–

[1] M. Stix, "On the time scale of energy transport in the sun," Solar Physics **212**, 3–6 (2003).

[2] E. H. Anders and B. P. Brown, "Convective heat transport in stratified atmospheres at low and high Mach number," Physical Review Fluids **2**, 083501 (2017), arXiv:1611.06580 [physics.flu-dyn].

[3] A. Brandenburg, K. L. Chan, Å. Nordlund, and R. F. Stein, "Effect of the radiative background flux in convection," Astronomische Nachrichten **326**, 681–692 (2005), astro-ph/0508404.

[4] E. A. Spiegel and G. Veronis, “On the Boussinesq Approximation for a Compressible Fluid.” Astrophys. J. **131**, 442 (1960).

[5] H. Johnston and C. R. Doering, “Comparison of Turbulent Thermal Convection between Conditions of Constant Temperature and Constant Flux,” Phys. Rev. Lett. **102**, 064501 (2009), arXiv:0811.0401 [physics.flu-dyn].

[6] N. E. Hurlburt, J. Toomre, and J. M. Massaguer, “Two-dimensional compressible convection extending over multiple scale heights,” Astrophys. J. **282**, 557–573 (1984).

[7] F. Cattaneo, N. H. Brummell, J. Toomre, A. Malagoli, and N. E. Hurlburt, “Turbulent compressible convection,” Astrophys. J. **370**, 282–294 (1991).

[8] L. Korre, N. Brummell, and P. Garaud, “Weakly non-Boussinesq convection in a gaseous spherical shell,” Phys. Rev. E **96**, 033104 (2017), arXiv:1704.00817 [physics.flu-dyn].

[9] K. Burns, G. Vasil, J. Oishi, D. Lecoanet, and B. Brown, “Dedalus: Flexible framework for spectrally solving differential equations,” Astrophysics Source Code Library (2016), ascl:1603.015.

[10] U. M. Ascher, S. J. Ruuth, and R. J. Spiteri, “Implicit-explicit Runge-Kutta methods for time-dependent partial differential equations,” Applied Numerical Mathematics **25**, 151–167 (1997).

[11] D. Lecoanet, B. P. Brown, E. G. Zweibel, K. J. Burns, J. S. Oishi, and G. M. Vasil, “Conduction in Low Mach Number Flows. I. Linear and Weakly Nonlinear Regimes,” Astrophys. J. **797**, 94 (2014), arXiv:1410.5424 [astro-ph.SR].

[12] B. Paxton, L. Bildsten, A. Dotter, F. Herwig, P. Lesaffre, and F. Timmes, “Modules for Experiments in Stellar Astrophysics (MESA),” The Astrophysical Journal Supplement Series **192**, 3 (2011), arXiv:1009.1622 [astro-ph.SR].